ON NEAR-FIELD GROUND MOTIONS OF NORMAL AND REVERSE FAULTS FROM VIEWPOINT OF DYNAMIC RUPTURE MODEL

Hideo AOCHI[1,2], Hiroe MIYAKE[3,4]

[1] Laboratoire de Géologie, Ecole Normale Supérieure/CNRS UMR 8538, PSL Research University, Paris, France

[2] BRGM, Orléans, France

[3] Center for Integrated Disaster Information Research, Interfaculty Initiative in Information Studies, The University of Tokyo, Japan

[4] Earthquake Research Institute, The University of Tokyo, Japan

E-mail contact of main author: aochi.hideo@gmail.com

Abstract. We report dynamic insights on mechanical differences in normal and reverse faults. The slip directions are simply opposite (rake of -90° and 90°) in kinematic description such that the ground motions can be symmetric, namely having an opposite sign in each component. However, does dynamic rupture process lead to the same result of slip history and ground shaking except for their polarity for the same given fault geometry (say, a fault dip of 45°) ? From the point of view of rupture dynamics, the problem is not symmetric when fault strength has normal stress dependency. We consider a normal or a reverse fault governed by the Mohr-Coulomb rupture criterion and followed by a slip-weakening friction during the rupture process. Reverse faulting can be accelerated when approaching to the ground surface, while normal faulting may be decelerated. This is because of the initial stress condition as well as dynamic stress perturbation. Considering this fact, for a given fault system, reverse fault setting may lead to an earthquake scenario more disastrous than normal fault, including allowing interaction between segments.

Key Words: Ground motion, Normal fault, Reverse fault, Dynamic rupture propagation.

1. INTRODUCTION

Anderson et al. [1] mentioned that ground motions in normal-faulting events are slightly smaller than in strike-slip or thrust events in several ground-motion prediction equations (GMPEs). Ground motions of normal faulting are not so largely recorded comparing to those of reverse faulting and strike-slip faulting, therefore the event term of normal faulting is still under discussion. The purpose of this paper is to demonstrate how the ground motions are different according to normal or reverse faulting from the point of view of rupture dynamics. In terms of kinematic description of earthquake source, ground motions are identical except the polarity when the same rupture scenario is given on a normal and reverse fault of the same fault geometry except for the rake (-90° or 90°). This means that the radiation pattern is symmetric for a given source. The point of this paper is to show that the rupture scenario cannot be the same for normal and reverse faults in the shallow when friction is supposed normal stress dependent (Coulomb friction). This has been known in dynamic rupture simulations [2-5]. Under the same condition, the rupture (fault slip) is made larger at the shallow depths on reverse fault than normal one due to the dynamic change of normal stress along the fault plane. In addition, increase of absolute stress with depth should be considered [6]. This is because the complexity of earthquake rupture in non-planar fault system, including here an interaction between the ground surface and fault, strongly depends on the absolute stress level [7].

There have been many attempts taking into account of dynamic rupture models in ground motion estimations, mostly focusing on the description of fault heterogeneity and slip time function [8-11]. These know-hows are practical levels of engineering applications for an assumed earthquake of a given magnitude. Another advantage is that dynamic rupture models are able to provide possible rupture scenarios under the known geological situations. For instance, expected earthquake size varies with the adopted fault geometry, assumed stress field and frictional parameters (e.g. [12]). Some of the scenarios may lead to an extremity, but this bias can be instead used for revising the probability of model parameters [13]. Nevertheless there have been few studies reporting on the influence of absolute stress on rupture process and ground motions.

In the following, we review the dynamic rupture models of an embedded shallow fault. Rupture process is perturbed dynamically during an earthquake but also is controlled in the initial condition. Namely normal and reverse faults cannot be loaded in the same way with the same frictional coefficients. We then compare the ground motion patterns in terms of the Peak Ground Velocity (PGV). We aim to study the difference in the ground motion prediction, which cannot be the same for normal and reverse faults.

2. METHOD AND MODELS

2.1. Numerical Method and Setting

We simulate ground motions as well as dynamic rupture process using Boundary Domaine Method (BDM), a hybrid scheme [14] combining a boundary integral equation in a homogeneous, infinite medium and a finite difference in a semi-infinite medium. BDM is able to introduce heterogeneity outside of the source volume, but we calculate here the ground motions in a homogeneous, semi-infinite medium in which the dynamic rupture models of our target have been previously simulated [6]. The model volume is prepared for 60 km (EW) x 60 km (NS) x 30 km (UD) in which a 45°-dip fault of 30.3 km x 13.8 km is embedded from 575 m to 10121 m depth (*FIG. 1*). We randomly distribute 441 receivers on ground surface (on average every 3 km). The resolution is controlled by finite difference scheme and the model parameters of simulations are summarized in *Table 1*.

TABLE 1: MODEL PARAMETERS USED FOR BDM.

Parameter	**Quantity and unit**
Grid spacing in finite difference *ds*	200 m
Time step in finite difference *dt*	0.00595 s
Medium density ρ	2800 kg/m^3
P- and S-wave velocities *Vp* and *Vs*	6300 m/s and 3637.3 m/s

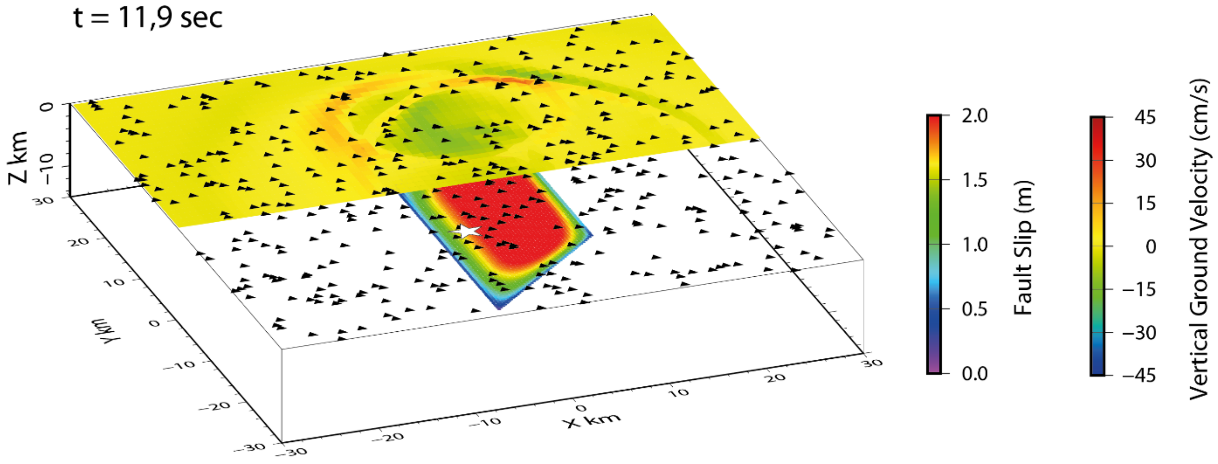

FIG. 1. Birdview of model setting in this study. The fault geometry and the receiver position (triangles) are common for all the simulations. Star represents the hypocenter position at (0, 0, -8 km). Vertical ground velocity and fault slip at 11.9 seconds is illustrated for a reverse fault under stress condition of Case 1.

2.2. Rupture Models

This section briefly explains the simulated rupture models [6]. For a fault of the fixed geometry, normal and reveres faulting are considered respectively under two different initial conditions. In all the cases, the rupture process is governed by the Coulomb and slip-weakening friction laws, namely

$$\tau_p = c + \mu_s \sigma_n \qquad \tau_r = \mu_d \sigma_n \qquad (1)$$

$$\tau(\Delta u) = \Delta\tau_b H(1-\Delta u / D_c)(1-\Delta u / D_c) \quad \text{where} \quad \Delta\tau_b = \tau_p - \tau_r \quad . (2)$$

Here τ_p and τ_r are peak and residual strength governed by cohesive force c, static and dynamic frictional coefficients μ_s and μ_d and effective normal stress σ_n. The transition of shear stress from τ_p to τ_r decreases linearly with on-going slip Δu until critical slip displacement D_c. $H(x)$ is the Heaviside step function and $\Delta\tau_b$ is called breakdown strength drop. *Table 2* summarizes the two model settings [6]. The dynamic rupture process is not symmetric on normal and reverse faults in both cases.

Case 1 – Uniform initial stress condition.

The same initial values of shear and normal stresses are given uniformly over the entire normal and reverse faults. Although the initial values are given a priori, the dynamic rupture process at each point follows *Equations* (1) and (2) according to the change of both shear and normal stresses during the rupture. Earthquake magnitude is smaller on normal fault than on reverse one. Normal stress increases after the strength drop on normal fault so that shear stress increases and vice versa on reverse fault.

Case 2 – Constrained depth-variable stress condition.

The initial stress field is given by principal stresses. Vertical principal stress is then set to the maximum for normal fault and minimum for reverse one, respectively. Confining pressure and hydrostatic pressure in the medium increase the vertical principal stress with depth. In this case, the initial stress on a fault is constrained by Mohr-circle, which is set as large as possible with respect the Coulomb friction lines, namely stress parameter *T* is 1 [13]. Stress accumulation becomes variable with depth. Earthquake scenarios are different for normal and reverse faults as the initial conditions are different. Furthermore, it is worth remarking that the initial stress cannot be loaded favorably at the shallowest part of normal fault (above 1 km depth). On the other hand, it can be loaded favorably up to zero depth. As a result, rupture is decelerated on normal fault in the shallow of normal fault, while is accelerated upward on reverse fault.

As a result, *FIG.2* characterizes the simulated four cases. Commonly in both cases, the peak of fault slip appears deeper on normal fault than reverse one. The difference of shallow behavior is observed in maximum slip rate distribution, which is smaller on normal fault, too. By the way, it is found that maximum slip rate is higher at depth for Case 2, because stress drop is also higher in the given situation.

TABLE 2: PARAMETERS FOR DYNAMIC RUPTURE MODELS AND CHARACTERISTICS OF SIMULATED RESULTS AFTER [6]. THE INITIAL CONDITION OF CASE 2 IS GIVEN BY CONSIDERING PRINCIPAL STRESSES, CONFINING AND HYDRO-STATIC PORE PRESSURES VARIABLE WITH DEPTH, CONSTRAINED STRESS PARAMETER T.

Parameter	**Case 1**	**Case 2**
Frictional coefficients μ_s and μ_d	0.6 and 0.4	0.6 and 0.45
Cohesive force c	0	5 MPa
Critical slip displacement Dc	0.2 m	0.8 m
Initial shear and normal stresses (σ_n, τ)	(50 MPa, 25 MPa)	Depth-variable.
Stress parameter T	-	1.0
Simulated magnitude Mw for normal/reverse faults	6.8 / 6.9	6.9 / 7.2

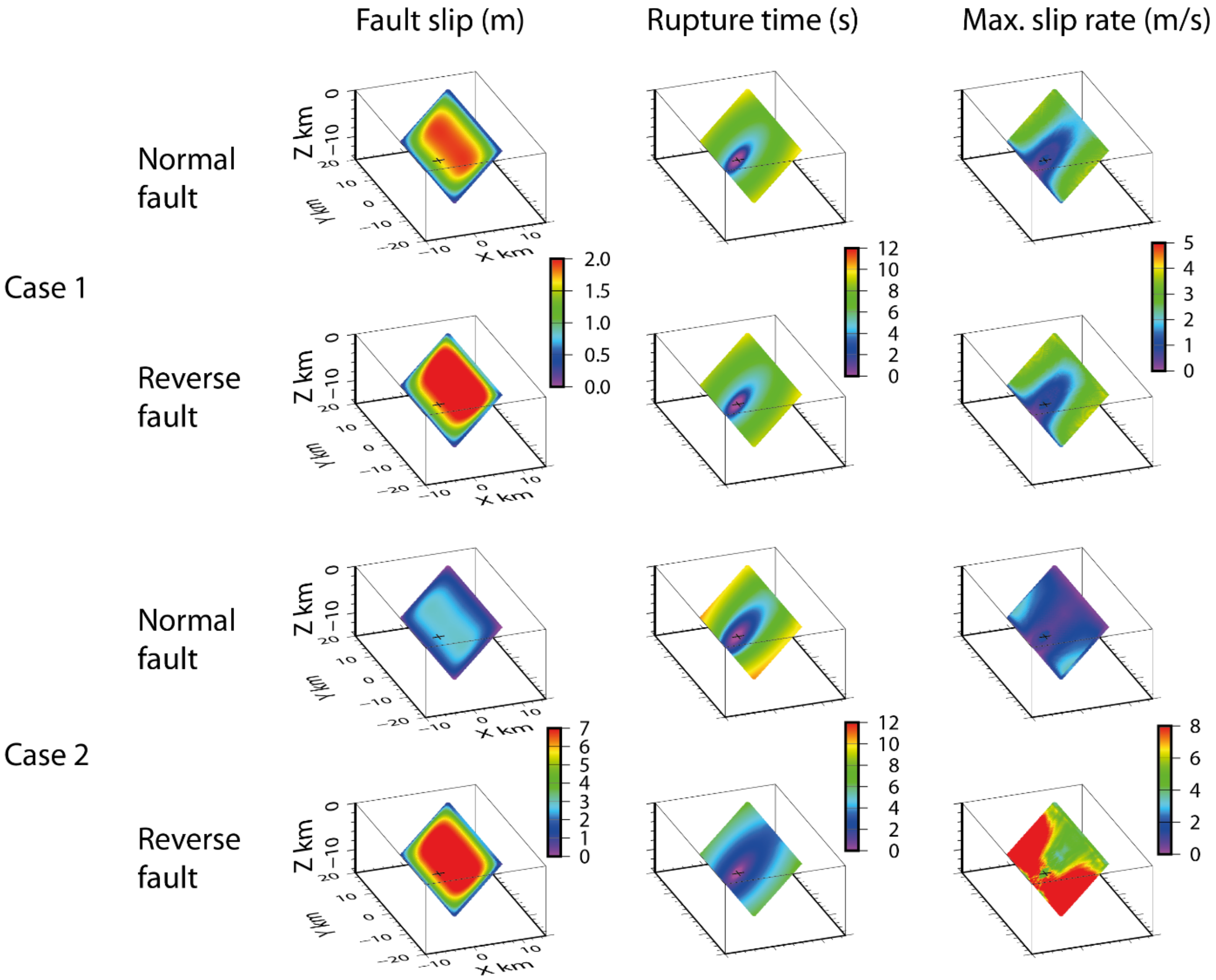

FIG.2. Summary of four simulations after [6]. A normal and reverse fault for two different stress cases, respectively. Case 1: Uniform initial stress. Case 2: Constrained depth-variable stress. Fault slip, rupture time and maximum slip rate at each point of the fault are illustrated. The color scales are different for the two cases.

3. Ground Motions

FIG.3 shows the Peak Ground Velocity (PGV) of each component on the ground surface. The rupture model is uniform without any additional heterogeneity such as asperities and ground motions are low-pass filtered up to 1 Hz. The fault geometry is the same for all the four cases. The fault plane is west-dipping. Strong ground motions appear at the eastern edge of the fault plane and on the hanging wall. A reverse fault of Case 1 and a normal fault of Case 2 have the same magnitude Mw6.9, however the amplitude in ground motions is larger in the former than the later.

We compare PGV of three components from the four cases in *FIG. 4*. When comparing them in each case, the ground motions are slightly larger for the reverse fault than for the normal one (Case 1), and get much larger (Case 2), according to the change of the stress field and therefore the rupture process (*FIG. 2*). Furthermore, the divergence of PGV at the near distance is particularly remarked for normal fault under Case 2, different from the other simulations. In the reverse fault, the PGV values uniformly increases at any distance from Case 1 to Case 2. This can be explained by the fact that the rupture process is similar although it becomes stronger due to higher stress drop and larger resultant magnitude in Case 2 than Case 1. However, for the normal fault, the magnitude increases slightly from Case 1 to Case 2, while the ground motions appear differently. First, no increase of ground motion levels is observed in Case 2. Second, the ground motions are significantly decreases at some receivers on the footwall at distance shorter than 10 km. These mean that the rupture process changes in detail between the two cases. The large slip remains at depth and it is considered that the shallow part of the normal fault does not contribute to seismic wave radiation in Case 2 due to the braking mechanism of normal faulting in which the shallow part cannot accumulated any tectonic stress from mechanical point of view [6].

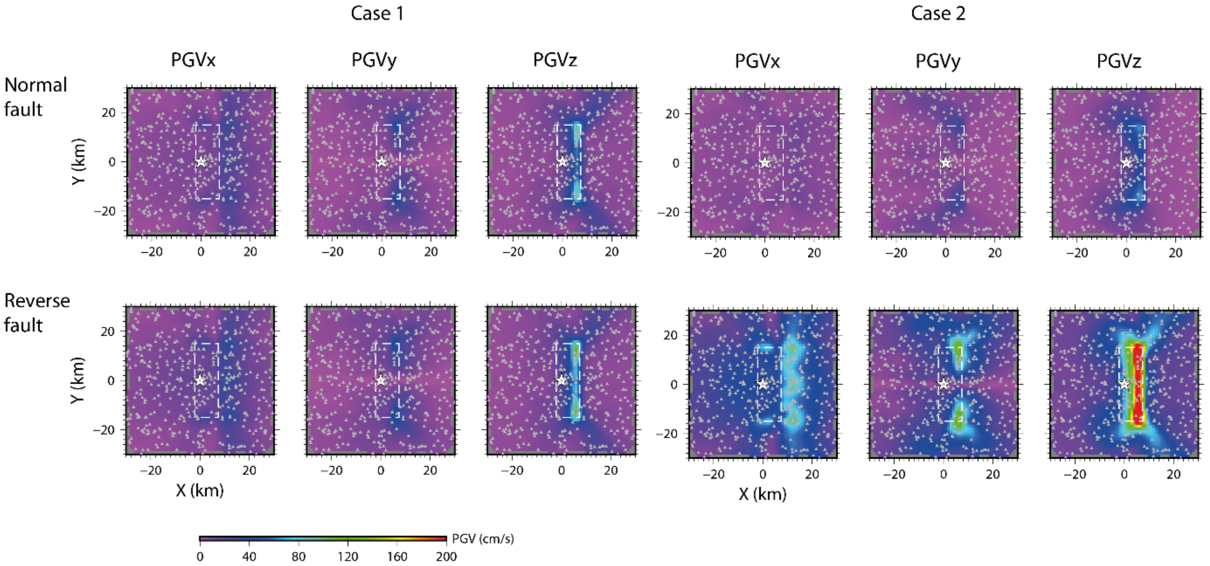

FIG.3. Peak Ground Velocity (PGV) of each component of ground motions for four dynamic rupture models presented in FIG.2. Ground motions are low-pass filtered up to 1 Hz. Star represents epicenter position, broken lines correspond to projected ruptured area, and small triangles are randomly distributed receivers.

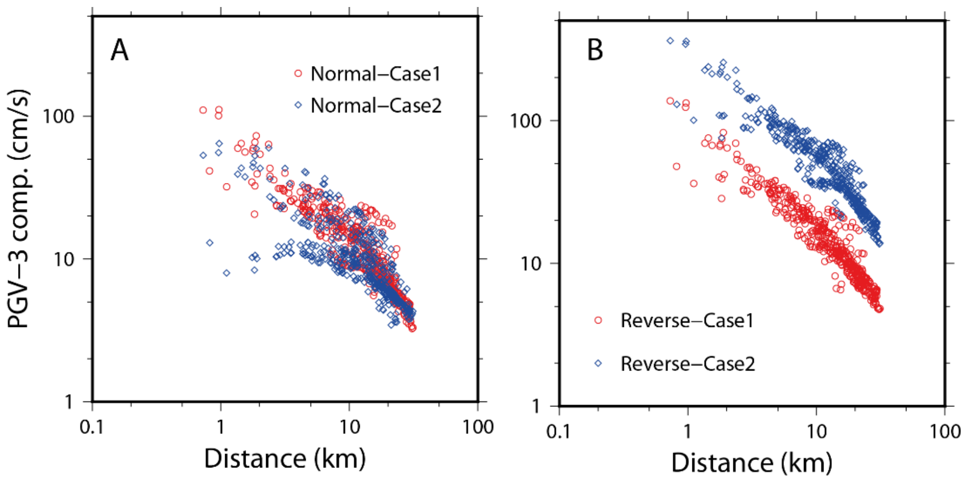

FIG.4. Peak Ground Velocity (PGV) of three-components in function of distance to the ruptured fault plane. Normal and reverse faults in panels A and B, respectively. PGV is calculated after low-pass filter up to 1 Hz. The 441 receiver positions are the same in FIGs 1 and 3.

4. Discussion and Conclusion

In this paper, we have demonstrated ground motions of shallow normal and reverse faults under different stress conditions. Supposing the same fault geometry, reverse faults becomes stronger and larger at the shallow depths due to the stress perturbation from the ground surface (Case 1). When a constrained depth-dependent stress accumulation is assumed (Case 2), the ground motions of the reverse fault are shifted higher uniformly, while those of the normal one is dissipated at the near distance (< 10 km). At some receivers, the ground motions become very weak. This is because that the rupture process is braked at the shallow depths of normal faulting, not only by the dynamic interaction of ground surface but also by the possible accumulation of initial stress level. As shown in the 2009 L'Aquila and 2016 Amatrice earthquakes, several normal-faulting events provide slip distribution with lateral extent from the hypocenter (e.g. [15-16]), and that may result in less ground motions on the footwall.

This difference is important for considering ground motion predictions. Once kinematic description of finite source is given, the ground motions are calculated in the same way for both normal and reverse faults and they are the same except for the polarity. However this study indicates that rupture scenarios cannot be the same in slip distribution and rupture velocity in terms of kinematic description. Our study is limited in the presented four simulations for a simple demonstration, however, it provides fundamental physical conditions for understanding rupture dynamics and related ground motions. It will be required to further explore the difference of seismological slip distribution and geological surface rupture between normal and reverse faults. For a site-specific study, it will be important to evaluate the stress accumulation in the shallow depths.

Acknowledgments

This work is contribution to the research project (Grant-in-Aide for Scientific Research B: grant 15H02989) from Japan Society for the Promotion of science (JSPS). The calculation is held at French national supercomputing center GENCI/CINES under the grant A0030406700 (2017-18).

REFERENCES

[1] ANDERSON, J. G. et al, "Ground otions in the Fukushima hamadori, Japan, normal-faulting earthquake", Bull. Seism. Soc. Am. **103** (2013) 1935-1951.

[2] NIELSEN, S. B., "Free surface effects on the propagation of dynamic rupture", Geophys. Res. Lett. **25** (1998) 125-128.

[3] OGLESBY, D. D. et al., Earthquakes on dipping faults: the effects of broken symmetry, Science **280** (1998), 1055-1059.

[4] OGLESBY, D. D. et al., "The three-dimensional dynamics of dipping faults", Bull. Seism. Soc. Am. **90** (2000) 616-628.

[5] RYAN, K. J., OGLESBY, D. D. "Modeling the effects of a normal-stress-dependent state variable, within the rate- and state-dependent friction framework, at stepovers and dip-slip faults", Pure Appl. Geophys. **174** (2017), 1361-1383.

[6] AOCHI, H., "Dynamic asymmetry of normal and reverse faults due to stress perturbation and constrained depth-dependent stress accumulation", submitted to Geophys. J. Int. (2018).

[7] AOCHI, H. et al., “Spontaneous Rupture Propagation on a Non-planar Fault in 3D Elastic Medium” Pure appl. Geophys. **157** (2000) 2003-2027.

[8] GUATTERI, M., et al., “Strong ground-motion prediction from Stochastic-dynamic source models”, Bull. Seism. Soc. Am. **93** (2003) 301-313.

[9] TINTI, E., et al., “A kinematic source-time function compatible with earthquake dynamics, Bull. Seism. Soc. Am. **95** (2005) 1211-1223.

[10] SONG, S. G., et al., "Pseudo-dynamic source modelling with 1-point and 2-point statistics of earthquake source parameters”, Geophys. J. Int. **196** (2014) 1770-1786.

[11] BAUMANN, C., DALGUER, L.A., "Evaluating the compatibility of dynamic rupture-based synthetic ground motion with empirical ground-motion prediction equation”, Bull. Seism. Soc. Am. **104** (2014) 634-652.

[12] ANDREWS, D. J., et al., "Physical limits on ground motion at Yucca Mountain” Bull. Seism. Soc. Am. **97** (2007) 1771-1792.

[13] AOCHI, H., et al. “Stress accumulation in the Marmara Sea estimated through ground-motion simulations from dynamic rupture scenarios”, J. Geophys. Res. **122** (2017) 2219-2235.

[14] GOTO, H. et al., “Simulation of spontaneous rupture based on a combined boundary integral equation method and finite element method approach: SH and P-SV cases” Geophys. J. Int. **183** (2010) 975-1004.

[15] CIRELLA, A., et al., “Rupture history of the 2009 L’Aquila (Italy) earthquake from non-linear joint inversion of strong motion and GPS data”, Geophys. Res. Lett. **36** (2009) L19304.

[16] TINTI, E. et al., “Slip heterogeneity and directivity of the M_L 6.0, 2016, Amatrice earthquake estimated with rapid finite-fault inversion”, Geophys. Res. Lett. **43** (2016) 10745-10752.